Antiviral Research 100 (2013) 259–268

Contents lists available at ScienceDirect

Antiviral Research

journal homepage: www.elsevier.com/locate/antiviral

Increased hydroxymethylglutaryl coenzyme A reductase activity during respiratory syncytial virus infection mediates actin dependent inter-cellular virus transmission

Laxmi Iyer Ravi [a], Li Liang [b], Pui San Wong [c], Gaie Brown [d], Boon Huan Tan [c], Richard J. Sugrue [a,b,*]

[a] Division of Molecular and Cell Biology, School of Biological Sciences, Nanyang Technological University, 60 Nanyang Drive, Singapore 637551, Singapore
[b] Singapore-MIT Alliance for Research & Technology (SMART), Centre for Life Sciences, 28 Medical Drive, Singapore 117456, Singapore
[c] Detection and Diagnostics Laboratory, DSO National Laboratories, 27 Medical Drive, Singapore 117510, Singapore
[d] MRC Virology Unit, Church St, Glasgow G11 5JR, UK

ARTICLE INFO

Article history:
Received 18 April 2013
Revised 26 June 2013
Accepted 19 August 2013
Available online 28 August 2013

Keywords:
Respiratory syncytial virus
Virus assembly
Actin
Virus transmission
Lovastatin
Hydroxymethylglutaryl coenzyme A reductase

ABSTRACT

We have examined the role that hydroxymethylglutaryl coenzyme A reductase (HMGCR) plays during respiratory syncytial virus (RSV) maturation. Imaging analysis indicated that virus-induced changes in F-actin structure correlated with the formation of virus filaments, and that these virus filaments played a direct role in virus cell-to-cell transmission. Treatment with cytochalasin D (CYD) prevented virus filament formation and virus transmission, but this could be reversed by removal of CYD. This observation, together with the presence of F-actin within the virus filaments suggested that newly polymerised F-actin was required for virus transmission. The virus-induced change in F-actin was inhibited by the HMGCR inhibitor lovastatin, and this correlated with the inhibition of both virus filament formation and the incorporation of F-actin in these virus structures. Furthermore, this inhibitory effect on virus filament formation correlated with a significant reduction in RSV transmission. Collectively these data suggested that HMGCR-mediated changes in F-actin structure play an important role in the inter-cellular transmission of mature RSV particles. These data also highlighted the interplay between cellular metabolism and RSV transmission, and demonstrate that this interaction can be targeted using anti-virus strategies.

1. Introduction

Human respiratory syncytial virus (RSV) is the most important cause of lower respiratory tract (LRT) infections in young children (Nair et al., 2010). This overall clinical scenario is worsened by the lack of an available effective vaccine and the limited availability and use of cost effective and specific antiviral drugs.

The mature respiratory syncytial virus (RSV) particle is surrounded by a lipid envelope in which the virus fusion (F) and attachment (G) virus glycoproteins are inserted. The F protein mediates fusion of the virus and host cell membranes during virus entry (Scheid and Choppin, 1977), while a primary role for the G protein is in virus attachment (Levine et al., 1987). The virus envelope surrounds a protein layer formed by the matrix (M) protein. This virus interior contains a ribonucleoprotein (RNP) complex formed by the viral genomic RNA (vRNA), the nucleocapsid (N) protein, phosphoprotein (P protein), M2-1 protein, and the large (L) protein (Grosfeld et al., 1995; Yu et al., 1995; Collins et al., 1996). During RSV infection two distinct virus structures are formed. The inclusion bodies are locations in the cell where the virus RNP-associated proteins and virus-specific RNA accumulate (Garcia et al., 1993; Garcia-Beato and Melero, 2000; Brown et al., 2005; Santangelo et al., 2006; Carromeu et al., 2007), suggesting that they may be sites of vRNA transcription and replication. Infectious virus particles with a filamentous morphology form on the plasma membrane (Roberts et al., 1995) and these are referred to as virus filaments.

The cellular processes involved in virus filament formation are still poorly understood, but the involvement of lipid-raft microdomains and F-actin in RSV morphogenesis has been suggested (Burke et al., 1998; Gower et al., 2001; Brown et al., 2002; Bitko et al., 2003; McCurdy and Graham, 2003; Gower et al., 2005; Kallewaard et al., 2005; Jeffree et al., 2007; Yeo et al., 2009; Radhakrishnan et al., 2010). Hydroxymethylglutaryl coenzyme A reductase (HMGCR) is a key regulatory enzyme in cholesterol biosynthesis (Brown et al., 1973; Osborne et al., 1987; Goldstein and Brown, 1990), and we have previously demonstrated increased

* Corresponding author at: Division of Molecular and Cell Biology, School of Biological Sciences, Nanyang Technological University, 60 Nanyang Drive, Singapore 637551, Singapore. Tel.: +65 63162889.
E-mail address: rjsugrue@ntu.edu.sg (R.J. Sugrue).

0166-3542/$ - see front matter © 2013 Elsevier B.V. All rights reserved.
http://dx.doi.org/10.1016/j.antiviral.2013.08.012

HMGCR gene expression during virus maturation (Yeo et al., 2009). We originally speculated that increased HMGCR expression may be directly related to changes in the composition of lipid-raft membranes during virus infection. However, several studies have also suggested a role for HMGCR in mediating F-actin re-modelling in the cell (Bifulco et al., 1993; Koch et al., 1997), and we have extended our previous findings to examine if the increased HMGCR activity facilitates virus transmission via actin-remodelling.

2. Materials and Methods

2.1. Cells and virus culture

The RSV A2 strain and HEp2 were used and virus infectivity measured as described previously (Radhakrishnan et al., 2010). Unless specified, cells were infected with RSV using a moi of 3 in DMEM + 2% FCS at 33 °C.

2.2. Antibodies and specific reagents

Anti-G (Abcam), anti-RSV (RCL3) (Novacastra Laboratories), anti-N (Rixon et al., 2004; McDonald et al., 2004), anti-F (Geraldine Taylor IAH, UK), anti-actin (Sigma Aldrich), anti-actinin (Santa Cruz Laboratories), phalloidin-FITC (Sigma Aldrich), phalloidin-AF 633 (invitrogen), anti-rabbit and anti-mouse IgG conjugated to either FITC (Signa Aldrich), cy3 and cy5 (Amersham) or Alexa488 and Alexa555 (invitrogen) were used in this study. Lovastatin (Calbiochem) was activated prior to use (Keyomarsi et al., 1991) and cells pre-treated with activated lovastatin (10 μM in DMEM) for 12 h prior to infection (Gower et al., 2001). Methyl-β-cyclodextrin and cholesterol-methyl cyclodextrin (Sigma Aldrich) were prepared in PBS and used at a final concentration of 5 mM for 1 h after which they were removed and replaced with maintenance media. Cytochalasin D (Sigma Aldrich) was prepared in DMSO at 1 mg/ml and used at 5 μg/ml.

2.3. Immunofluorescence microscopy

Cells on 13 mm glass coverslips were fixed and stained with the relevant primary and secondary antibodies as described previously (Brown et al., 2002). The stained cells were mounted on slides using Citifluor and visualized using either a Nikon eclipse 80i fluorescence microscope, or a Zeiss Axioplan 2 confocal microscope using appropriate machine settings (Nikon ECLIPSE TE2000-U).

2.4. Scanning electron microscopy (SEM)

HEp2 cells were grown on glass coverslips (10 mm diameter) and processed as described previously (Jeffree et al., 2003). The cells were critically point-dried (Polaron CPD) prior to mounting on aluminium stubs and carbon-coated using an Edwards sputter coater device. The cells were visualized with a Jeol 5600 using appropriate machine settings.

2.5. Surface protein labelling

This was performed using 0.5 mg/ml sulpho-NHS-LC-LC-biotin (Pierce) as described previously (Low et al., 2008).

2.6. SDS PAGE and Western blotting

This was performed as described previously (Brown et al., 2005). The protein bands were visualized using the ECL protein detection system (Amersham, USA). In all cases the apparent molecular masses were estimated using Kaleidoscope protein standards (Bio Rad, USA).

2.7. Cytotoxicity and cholesterol measurements

Cytotoxicity measurements were performed using the cytotoxicity detection kit, LDH ver 8 (Roche), and cholesterol levels were quantified using the Amplex red cholesterol assay (Invitrogen) as recommended by the manufacturer. Absorbance values were measured using a Tecan Infinite F200 microplate reader with i-Control software and using appropriate machine settings and wavelengths.

3. Results and discussion

3.1. Virus-induced changes in F-actin structure plays a direct role in RSV particle assembly

Mock-infected and RSV-infected cells were stained using phalloidin-AF633 (detects F-actin) and visualised by fluorescence scanning confocal microscopy (FSCM) (Fig. 1A and B). Filamentous projections on mock-infected cells were consistent with F-actin stabilized membrane structures (e.g. microvilli) (Fig. 1A), while increased filamentous staining at the cell surface and at cell-to-cell contacts was observed in virus-infected cells (Fig. 1B). Infected HEp2 cells were labelled using phalloidin-AF633, anti-F and anti-G which recognize the virus surface proteins (indicates the presence of virus filaments) and imaged using FSCM which revealed a filamentous staining pattern in each case (Fig. 1C). Extensive co-localisation of the anti-G and phalloidin-AF633 along the entire length of the virus filaments was observed (Fig. 1D(i)), while the F protein staining was more apparent at the distal ends of the virus filaments (Fig. 1D(ii) and (iii)). RSV-infected cells were also co-stained using anti-N (indicates the presence of inclusion bodies and virus filaments), anti-F and phalloidin-AF633 to determine the relative distribution of the virus filaments, inclusion bodies and F-actin. Extensive co-localization of the N protein and F-actin at the cell top (Fig. 1E(i)), and periphery (Fig. 1E(ii)) was observed, while F protein staining at the ends of the virus filaments was again apparent (Fig. 1F(i) and (ii)). F-actin was not detected within the inclusion bodies suggesting that it is either not a major component of inclusion bodies, or that phalloidin-AF633 cannot penetrate the inclusion bodies.

3.2. Virus filaments mediate transmission by direct cell-to-cell contact

Virus filaments are cell-associated and virus transmission by direct contact between infected and non-infected cells would be expected. To confirm this, confluent HEp2 cell monolayers were infected using a multiplicity of infection (moi) of between 0.1 and 0.0001, and at 30 hpi the distribution of anti-RSV labelled cells was determined using immunofluorescence (IF) microscopy (Fig. 2A). A moi of 0.1 was sufficient to infect all cells in the monolayer by 30 hpi, while virus-infected cell clusters were visible on monolayers infected with a moi of 0.001 and 0.0001. These infected cell clusters accounted for >95% of the detectable staining on the monolayer and contained approximately 58 ± 10 infected cells per cluster, suggesting localized spreading of virus filaments in the cell monolayer.

Cells were infected using a moi of 0.05 and at 40 hpi infected cells clusters were detected (Fig. 2B). The tissue culture supernatant (TCS) was harvested (cell-free virus fraction) and cell-associated virus fraction was recovered by releasing the virus from the infected cells. Newly plated cell monolayers were challenged with each fraction and the presence of infected cells detected using IF microcopy. We failed to detect infectious virus in the TCS, while

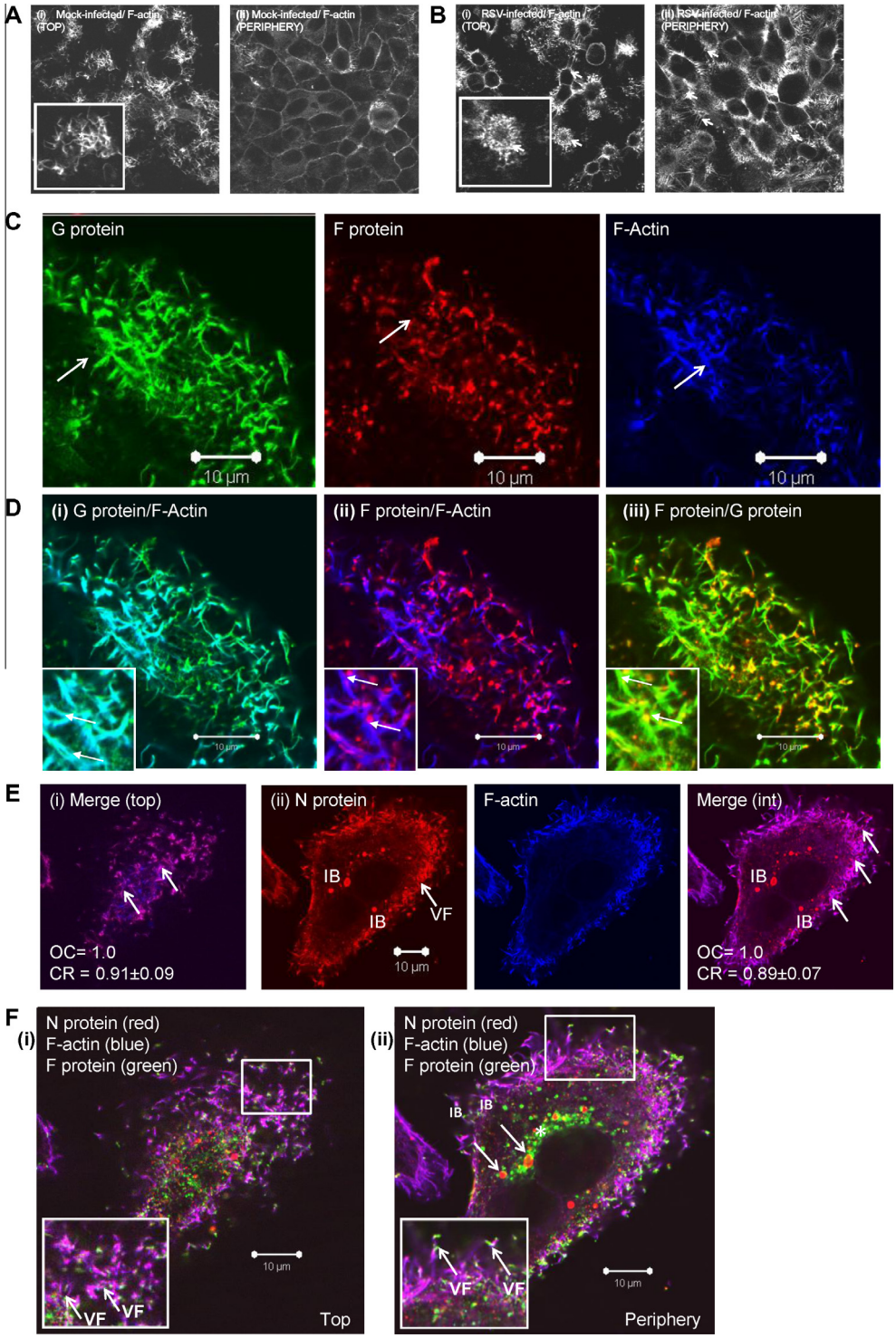

Fig. 1. RSV-induced changes in F-actin structure correlate with virus filament formation. At 18 h post-infection (hpi) (A) mock-infected and (B) RSV-infected cells were labelled with phalloidin-AF633 and imaged using fluorescence scanning confocal microscopy (FSCM) at optical planes showing (i) the cell top (TOP) and (ii) cell periphery (PERIPHERY). Inset, the F-actin structures are highlighted on mock-infected (∗) and virus-infected (white arrows) cells. (C) At 18 h post-infection (hpi) RSV-infected cells were labelled with anti-G (FITC; green), anti-F (cy3; red) and phallodin-AF633 (blue; F-actin) and the individual staining patterns were imaged using FSCM at a single optical plane that shows the virus filaments. (D) The relative distribution of the (i) G protein and F-actin, (ii) the F protein and F-actin, and (iii) the F and G proteins are also shown. Inset, areas of high co-localisation are highlighted (white arrows). (E and F) The relative distributions of F-actin, virus filaments (VF) and inclusion bodies (IB) in virus-infected cells are shown. At 18 hpi RSV-infected cells were labelled with anti-N (cy3; red), anti-F (FITC; green) and phalloidin-AF633 (blue; F-actin) and imaged using FSCM. (E) (i) the N protein and F-actin staining pattern in the merged image at the cell top (top) and (ii) the individual staining pattern for the N protein and F-actin at cell periphery (int) and are shown. The virus filaments (white arrows) and inclusion bodies (IB) are highlighted in the merged images. (F) The relative distribution of the F protein, N protein and F-actin. The stained cells were imaged using FSCM at a single optical plane at the (i) cell top (Top) and (ii) cell periphery (Periphery) of infected cell. The inclusion bodies (IB) are highlighted. Insets, the areas of enhanced F protein staining at the distal ends of the virus filaments are also highlighted (white arrow). The values of the overlap coefficient (OC) and correlation coefficient (CR) are indicated. (For interpretation of the references to colour in this figure legend, the reader is referred to the web version of this article.)

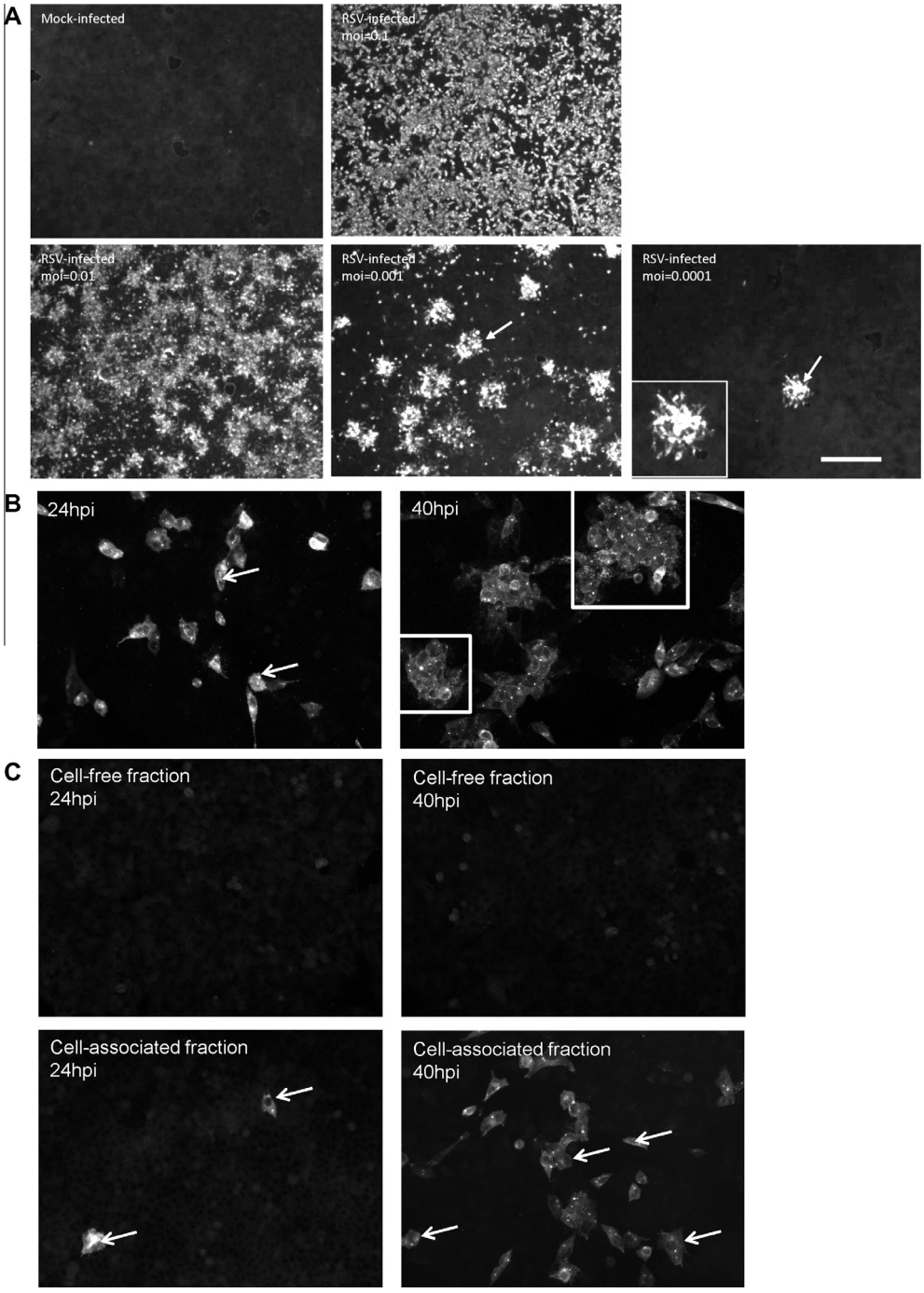

Fig. 2. RSV transmission occurs by direct cell-to-cell contact via virus filaments. (A) Near confluent HEp2 monolayers were infected with RSV using a multiplicity of infection (moi) of between 0.1 and 0.0001 and at 30 h post-infection (hpi) the cells were labelled with anti-RSV (Alexa 488) and the cell monolayers imaged using fluorescence microscopy (bar = 100 μm). (B and C) Cells were infected with RSV using a moi of 0.05 and (B) at 24 and 40 hpi the cell were stained using anti-RSV and viewed by fluorescence microscopy at magnification 20×. The single cells early in infection (white arrow) and infected cells clusters (white boxes) are indicated. (C) The relative levels of RSV infectivity associated with the tissue culture supernatant (TCS) (Cell-free fraction) and the cell-associated virus (Cell-associated fraction) was examined. HEp2 cells were infected using a moi 0f 0.05 and at 40 hpi the TCS was carefully harvested. The same volume of fresh DMEM was added to the cells monolayer and the cells harvested using a cell scraper. The virus was released from the cells by using a sonicating water bath at 4 °C (5 × 1 s pulses at low power at 5 min intervals). Both fractions were clarified by centrifugation to remove any insoluble material and added to HEp2 cell monolyers. At 20 hpi the cells were stained using anti-RSV to detect the presence of infected cells and imaged by fluorescence microscopy (magnification 20×).

relatively high level of cell-associated virus fraction was detected (Fig. 2C), with an estimated virus titer of approximately 8×10^4 pfu/ml.

HEp2 cell monolayers were infected with RSV using a moi of 0.05 and at 24 hpi the cells were labelled with anti-G and anti-α-actinin (to stain individual cells within the monolayer) and examined by FSCM. Virus filaments spreading from the initial point of infection to the surrounding non-infected cells was consistent with direct cell-to-cell transmission via the virus filaments (Fig. 3(i)–(iv)). The distal end of the virus filaments, where the F protein is

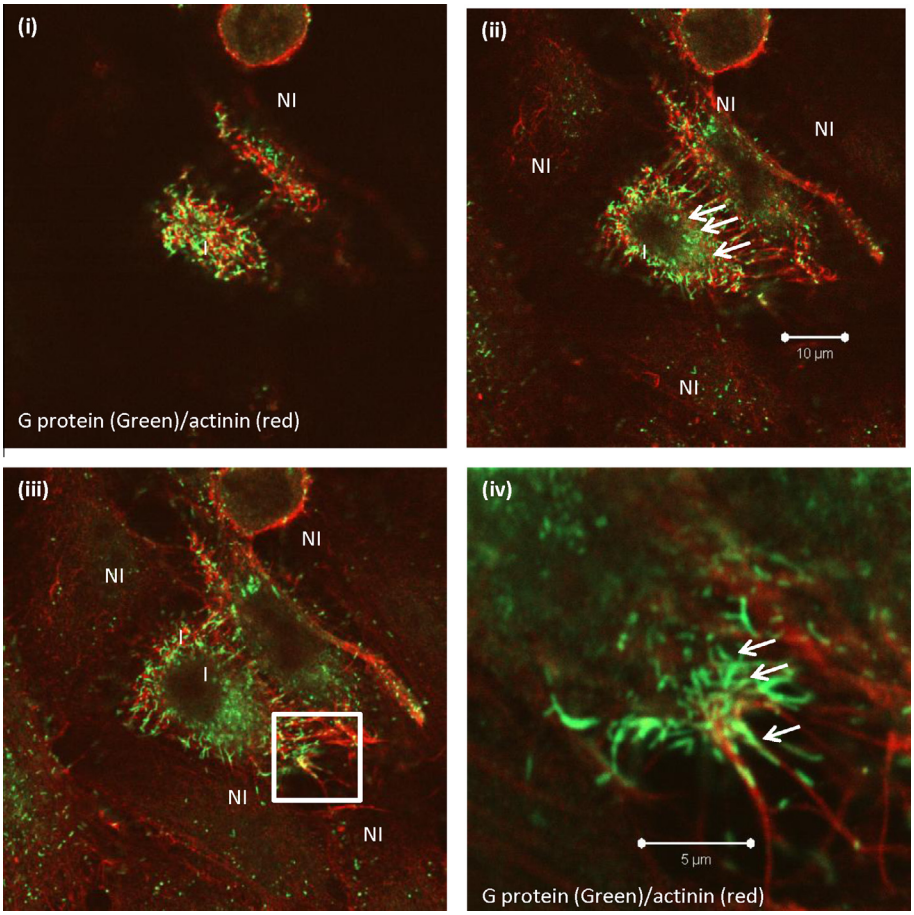

Fig. 3. Examination of cell-to-cell transmission by fluorescence scanning confocal microscopy (FSCM). Cells were infected using a moi of 0.2 and at 24 hpi the cells were stained using anti-actinin (cy3; red) and anti-G (FITC; green). The cells were imaged by FSCM at three optical planes from (i) the cell top to (iii) the cell periphery. The virus filaments (highlighted by white arrows) extending from infected cells (I) to non-infected cells (NI) are indicated. (objective 64×). (iv) shows an enlarged image from the boxed area in plate (iii). (For interpretation of the references to colour in this figure legend, the reader is referred to the web version of this article.)

concentrated (Fig. 1F(i) and (ii)), presumably makes contact with the surface of the non-infected cell during the initial stages of membrane fusion.

3.3. Actin polymerization is required for RSV transmission

The data suggested that F-actin polymerization may play a direct role in virus transmission, and this possibility was examined further using the actin polymerization inhibitor cytochalasin D (CYD). Virus filaments start to form by 12 hpi (Yeo et al., 2009), and infected cells were either non-treated (NT) or CYD-treated from 9 hpi (i.e. prior to the onset of virus filament formation). At 18 hpi the cells were labelled with anti-G (Fig. 4A) and phalloidin-FITC (Fig. 4B) and imaged using FSCM. The NT-treated cells exhibited a predominantly filamentous anti-G staining pattern (Fig. 4A(i)), and although similar G protein labelling intensity was observed in CYD-treated cells, a change to a punctate labelling pattern was noted (Fig. 4A(ii)). A loss in the filamentous phalloidin-FITC staining pattern in CYD-treated cells was consistent with F-actin destabilization (Fig. 4B).

The effect of CYD treatment on virus transmission was examined on near confluent monolayers infected with RSV using a moi of 0.05 (Fig. 4C). At 18 hpi the cells were either non-treated or CYD-treated, and at 30 hpi the anti-G stained monolayers were examined by IF microscopy. Non-treated cell monolayers exhibited infected cell clusters, while brightly labelled single-infected cells were observed on CYD-treated cell monolayers. Removal of the CYD at 24 hpi was sufficient to restore RSV transmission by 30 hpi in a similar manner to that in non-treated cells. These data support a role for newly polymerized actin in the process of RSV filament formation and cell-to-cell transmission.

We examined if CYD treatment could mediate release of virus. Cells were infected using a moi of 3 and at 24 hpi the infection confirmed (Fig. 4D(i) and Fig. 4E(ii)). Cell-associated virus was detected in the non-treated and CYD-treated cells, accounting for virus titers of 0.9×10^5 and 6.2×10^5 pfu/ml, respectively. Only sporadic staining was observed in the cell-free virus of non-treated cells was observed at moi of 3 (representing approximately 0.1% of the plated cells (Fig. 4D(ii) and Fig. 4E(ii)). Using a moi of 0.05 in either non-treated or CYD-treated cells only cell-associated virus was detected.

3.4. Hydroxymethylglutaryl coenzyme A reductase (HMGCR) activity mediates virus-induced F-actin remodelling and RSV filament formation

We have previously demonstrated increased expression of HMGCR and several other genes that play a role in cholesterol biosynthesis during virus filament formation (Yeo et al., 2009). Increased expression of these genes would be expected to lead to increased cholesterol levels during virus infection. We compared the cholesterol levels in mock and virus-infected cells at 18 hpi which indicated an approximate 30% increase in cholesterol levels following RSV infection (Fig. 5A), consistent with our earlier gene expression analysis.

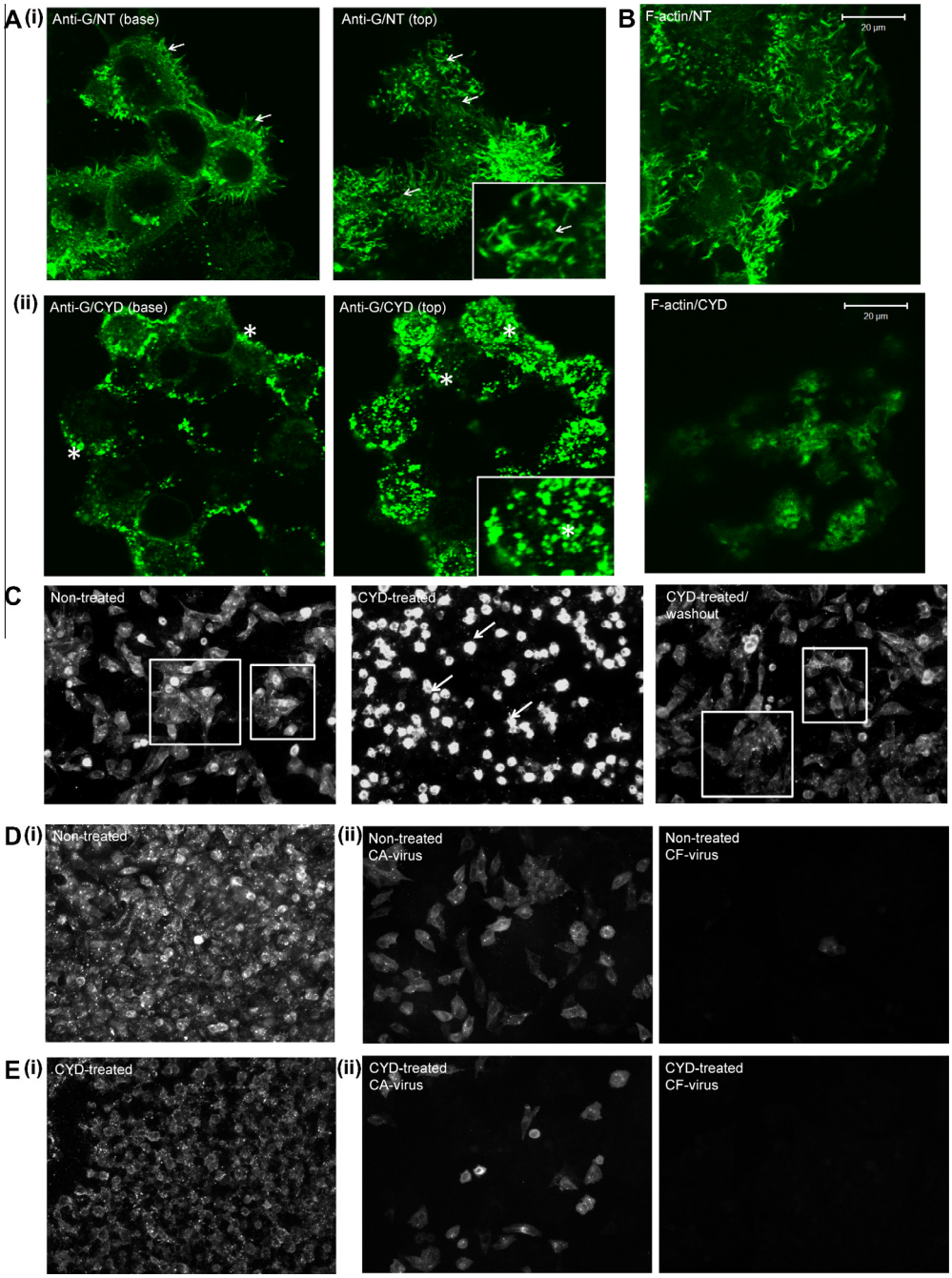

Fig. 4. RSV requires newly polymerized actin for cell-to-cell transmission. (A) Cells were infected with RSV and at 9 h post-infection (hpi) the cells were either (i) non-treated (NT) or (ii) cytochalasin-D-treated (CYD). At 18 hpi the cells were labelled with anti-G (Alexa488; green) and imaged using fluorescence scanning confocal microscopy (FSCM) at a focal plane that allows the cell periphery (periphery) and cell top (top) to be visualized. The virus filaments (white arrows) and punctate staining patterns (∗) are highlighted. Insets are enlarged images of virus-infected cells showing the distinct staining patterns. (B) Non-treated (NT) and cytochalasin-D-treated (CYD) cells were also stained using phalloidin-FITC. (C) Actin polymerization is required for cell-to-cell transmission. Cells were infected with RSV using a multiplicity of infection of 0.2 and at 18 hpi either non-treated or cytochalasin-D-treated (CYD-treated). At 24 hpi the cytochalasin-D was removed from some infected cultures (CYD-treated/washout). In all cases at 30 hpi the cells were labelled with anti-RSV and the cells visualized using a Nikon eclipse 80i fluorescence microscope in fluorescence microscopy mode (objective 20×). The infected cell clusters (white box) and individual stained infected drug-treated cells (white arrow) are highlighted. (D and E). RSV-infected cells were infected using a moi of 3 and at 8 hpi the cells were either non-treated or CYD-treated. At 24 hpi the cells were either (D(i) and E(i)) stained using anti-RSV and examined immunofluorescence microscopy or (D(ii) and E(ii)) the cells separated into cell-associated (CA) and cell-free (CF) fractions and the resulting preparations used to infect HEp2 cells. After 24 hpi the cells were stained using anti-RSV and imaged by immunofluorescence microscopy. (For interpretation of the references to colour in this figure legend, the reader is referred to the web version of this article.)

A role for HMGCR activity in F-actin re-modelling has been proposed (Bifulco et al., 1993; Koch et al., 1997), and we used the HMGCR inhibitor lovastatin to examine if HMGCR activity played a role in F-actin remodelling during virus morphogenesis. HEp2 cells treated with between 1 and 50 μM lovastatin exhibited no significant cytotoxic effect under our experimental conditions (Fig. 5B), and in subsequent experiments when appropriate cells were treated using 10 μM lovastatin. The cholesterol levels in lovastatin-treated virus-infected cells were similar to that in mock-infected cells (Fig. 5A). Although lovastatin prevented the

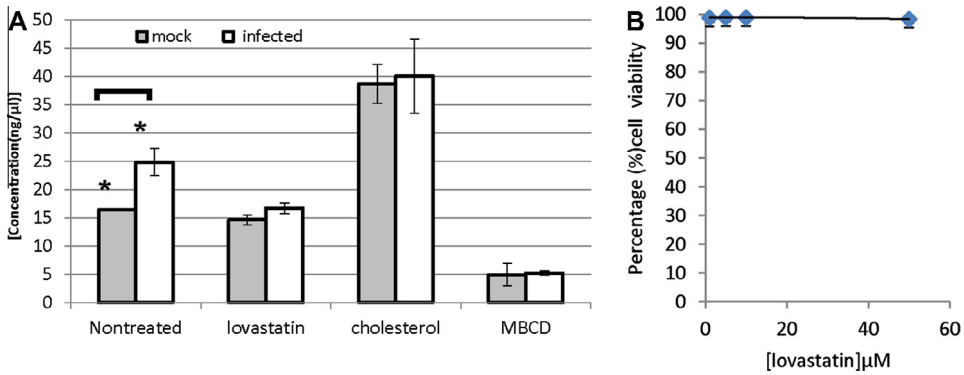

Fig. 5. Biochemical evidence for increased HMGCR activity during RSV infection. (A) RSV-induced increased HMGCR activity is inhibited by lovastatin treatment. Mock and RSV-infected cells were either non-treated, lovastatin-treated (Lovastatin), or with cholesterol-methyl-β-cyclodextrin-treated (cholesterol) or Methyl-β-cyclodextrin-treated (MBCD) between 7 and 8 h post-infection (hpi). At 18 hpi the free-cholesterol levels were measured. The values obtained are averages or triplicate measurements and representative data from one of two separate experiments is shown ($P < 0.05$). (B) Cytotoxicity measurements (percentage cell viability) from HEp2 cells treated with increasing lovastatin concentrations (μM) for 30 h. The values obtained are averages of triplicate measurements and representative data from one of two separate experiments is shown. ($P < 0.05$).

virus-induced cholesterol biosynthesis it did not reduce the basal cellular cholesterol levels; consistent with the inhibition of the increased HMGCR activity during virus infection.

Mock-infected and non-treated or lovastatin-treated RSV-infected HEp2 cells were labelled with phalloidin-FITC (Fig. 6) and the F-actin staining pattern examined by IF microscopy. This confirmed the virus-induced changes in the F-actin staining pattern following virus infection, but this change in F-actin was not observed in lovastatin-treated infected cells. This indicated that lovastatin-treatment inhibited the virus-induced changes in F-actin, and we examined the effect of lovastatin treatment on virus filament formation.

Non-treated and lovastatin-treated RSV-infected HEp-2 cells were labelled with anti-G and examined by FSCM (Fig. 7A). The surface of non-treated infected cells exhibited numerous virus filaments, while in lovastatin-treated cells which was replaced by a staining pattern that varied between stunted filaments to punctate in appearance. This suggested impaired virus assembly in lovastatin-treated cells, which was confirmed using scanning electron microscopy (SEM). As expected, numerous virus filaments were observed on the surface of non-treated cells (Parry et al., 1979; Roberts et al., 1995; Jeffree et al., 2003, Brown et al., 2004), while lovastatin-treated infected cells exhibited a surface topology that was similar to that of mock-infected cells (Fig. 7B). The effect of drug treatment on the surface expression of the F and G proteins was examined by immunoprecipitation of surface-biotinylated non-treated and lovastatin-treated infected cells detergent extracts with anti-F and anti-G (Fig. 7C). Similar levels of surface-labelled F and G proteins were detected in non-treated and lovastatin-treated infected cell lysates, indicating that drug-treatment did not impair transport of these proteins to the surface of infected cells. We can therefore conclude that the altered staining pattern observed on lovastatin-treated cells may represent the sites of RSV assembly. During infection it would be expected that F-actin remodelling mediates the extension of these structures that give rise to the more accentuated filamentous staining pattern that is characteristic of virus filaments.

The distribution of the F-actin and virus filaments in non-treated and lovastatin-treated virus-infected cells was compared using FSCM. Although co-staining of F-actin and the G protein within virus filaments on non-treated infected cells was observed (Fig. 8A), this co-staining pattern was significantly reduced in lovastatin-treated infected cells (Fig. 8B); as indicated by a reduction in the correlation coefficient values in lovastatin-treated cells. This suggested that lovastatin treatment impaired virus filament formation by inhibiting the virus-induced changes in the F-actin structure that correlated with the incorporation of F-actin in the virus filaments.

3.5. Hydroxymethylglutaryl coenzyme A reductase (HMGCR) activity is required for RSV transmission

Since HMGCR activity is required for virus filament formation we examined the effect of lovastatin on virus transmission in confluent HEp2 cell monolayers. Non-treated and lovastatin-treated HEp2 monolayers were infected with RSV using a moi of 0.1, and at 36 hpi the distribution of infected cells examined. The cell monolayers were stained using anti-G and examined using bright-field

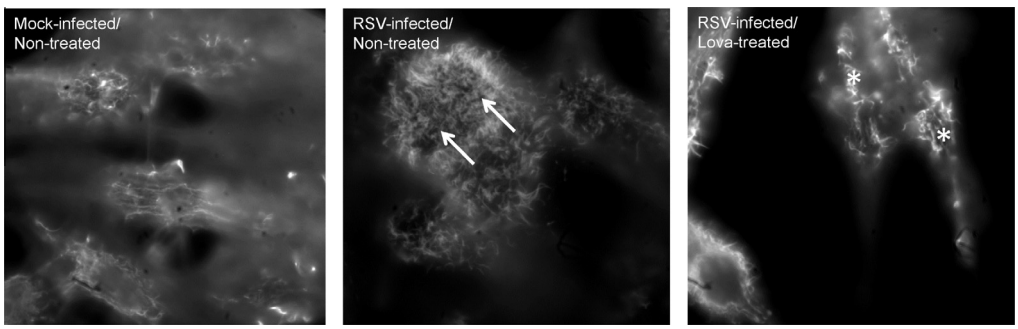

Fig. 6. Lovastatin inhibits virus-induced change in the F-actin network. At 18 h post-infection (hpi) mock-infected and virus-infected non-treated or virus-infected lovastatin-treated (Lova-treated) cells were stained using phalloidin-FITC and imaged by fluorescence microscopy using identical camera settings. The increased filamentous staining pattern following RSV infection is shown (white arrows), while the F-actin staining pattern in lovastatin-treated virus infected cells is highlighted (*).

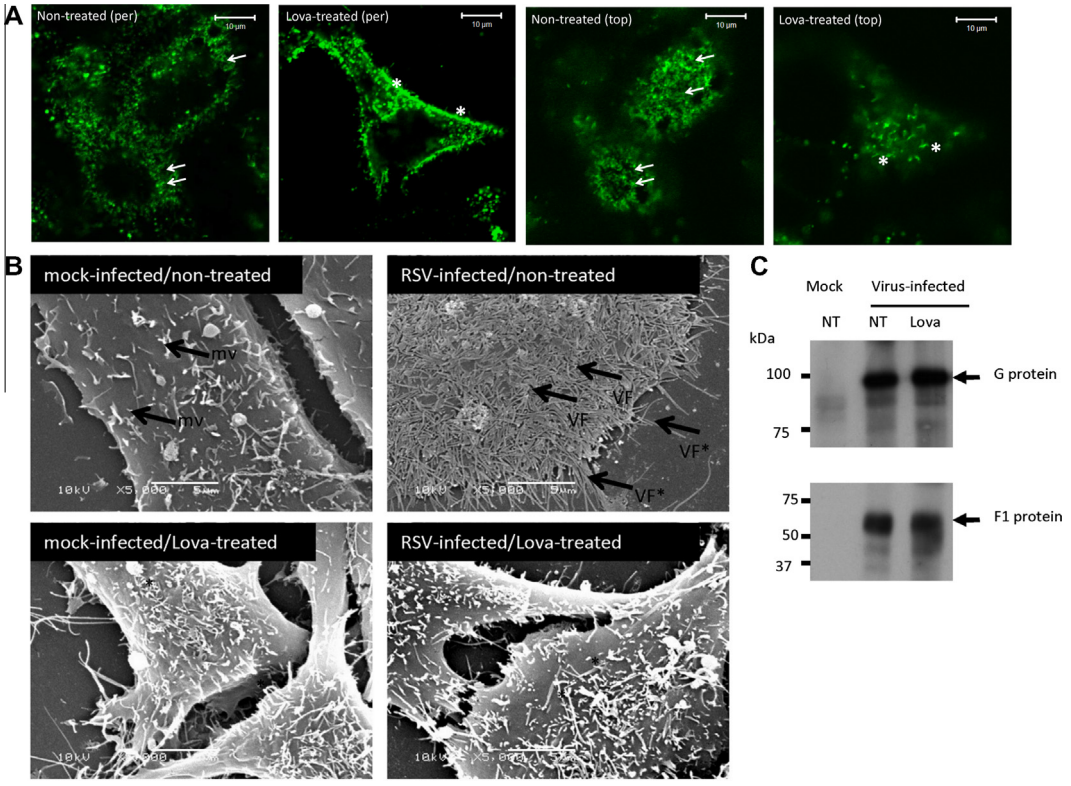

Fig. 7. Lovastatin inhibited virus filament formation. (A) RSV-infected cells were either non-treated or lovastatin-treated (Lova-treated) and at 18 h post-infection (hpi) the cells labelled with anti-G (FITC, green). The stained cells were examined by fluorescence scanning confocal microscopy (FSCM) at optical planes representing the cell surface (sur) or cell periphery (int). The virus filaments (VF) and the predominant punctate staining pattern in Lova-treated cells (*) are highlighted. (B) Mock and RSV-infected cells were either non-treated or Lova-treated, and at 18 hpi the cells were visualized using scanning electron microscopy (SEM) at magnification 5000×. The surface features on mock-infected cells (black arrow) and the virus filaments (VF) on RSV-infected cells are highlighted. Also shown are virus filaments radiating from the cell periphery (VF*). (C) Mock-infected cells and virus-infected cells either non-treated (NT) or lovastatin-treated (Lova) were surface-biotinylated. At 18 hpi the surface expressed F and G protein isolated by immunoprecipitation and analyzed as described in methods. Protein species of the correct size of the G protein (90 kDa) and F1 protein (55 kDa) are indicated. (For interpretation of the references to colour in this figure legend, the reader is referred to the web version of this article.)

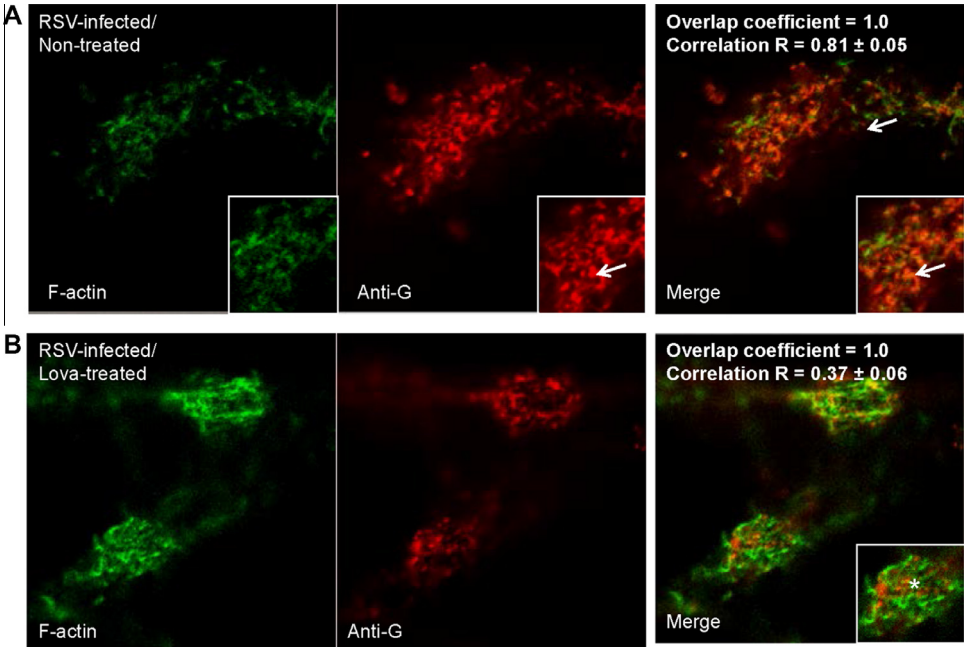

Fig. 8. The effect of lovastatin treatment on virus-associated F-actin. (A) Non-treated or (B) Lova-treated infected cells were stained using phalloidin-FITC (green) and anti-G (Alexa555; red) and imaged using FSCM (objective 100×). The virus filaments (white arrows) in non-treated cells and the punctate staining pattern (*) in Lova-treated cells are highlighted. The values of the overlap coefficient and correlation R are indicated. (For interpretation of the references to colour in this figure legend, the reader is referred to the web version of this article.)

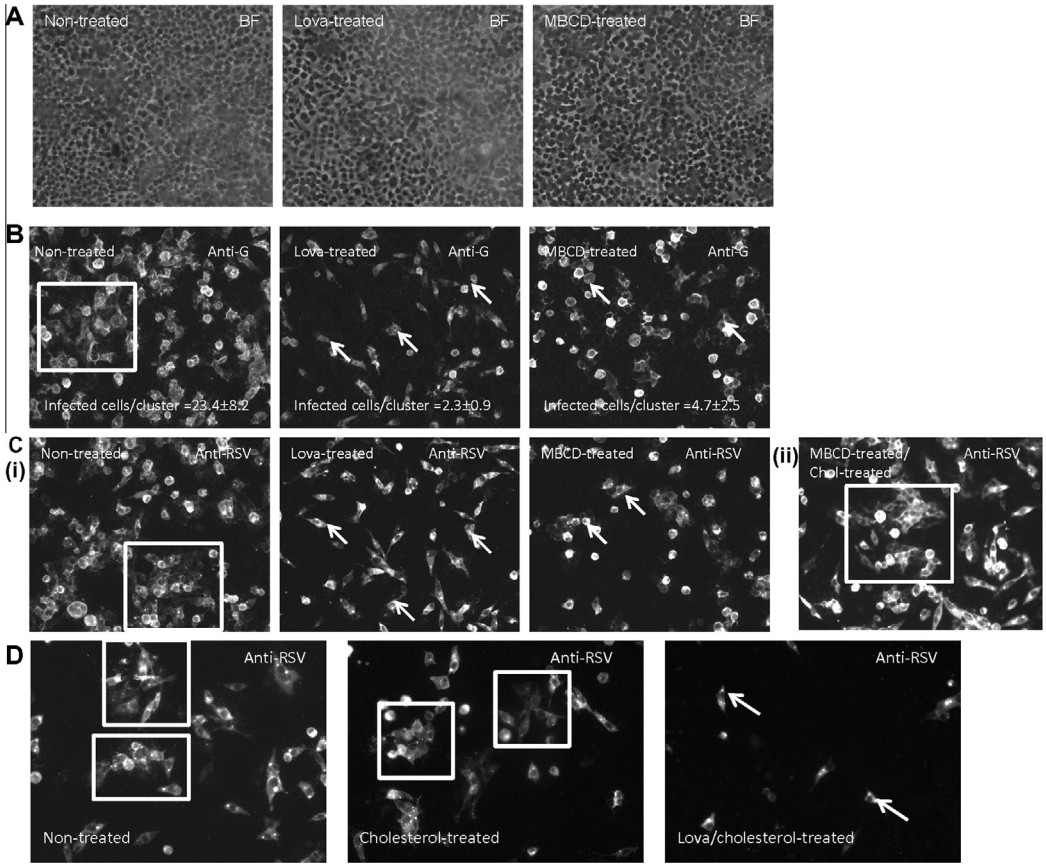

Fig. 9. Hydroxymethylglutaryl coenzyme A reductase (HMGCR) activity is required for virus cell-to-cell transmission. HEp2 cell monolayers were infected with RSV using a multiplicity of infection of 0.05 and were either non-treated, lovastatin-treated (Lova-treated) from 12 hpi, or Methyl-β-cyclodextrin-treated (MBCD-treated) from between 18 and 19 hpi. At 30 hpi the cells were labelled using anti-G or anti-RSV. The anti-G stained cells were imaged using (A) bright-field (BF) and (B) fluorescence microscopy and the average number of infected cells per infected cell cluster is shown, while (C(i)) the anti-RSV stained cells were imaged using fluorescence microscopy. (C(ii)) cells were MBCD-treated from between 18 and 19 hpi, and then treated with cholesterol-methyl-β-cyclodextrin (ch-MBCD) between 19 and 20 hpi. At 30 hpi the cells were stained using anti-RSV and imaged using fluorescence microscopy. (D) Infected cells were either non-treated, ch-MBCD-treated (cholesterol-treated), or lovastatin-treated and then treated with ch-MBCD (Lova/cholesterol treated). At 30 hpi the cells were labelled with anti-RSV and imaged using fluorescence microscopy. Lovastatin treatment was maintained throughout and the ch-MBCD was added at between 19 and 20 hpi. The stained cells were visualized using a Nikon eclipse 80i fluorescence microscope (objective 20×). Large clusters of infected cells in non-treated cells (in white box) and the singly stained infected cells (white arrow) are highlighted.

(BF) and IF microscopy. BF microscopy showed similar cell densities in non-treated and lovastatin-treated cells indicating that the cell numbers remained unchanged following drug treatment (Fig. 9A). In anti-G stained non-treated cells we observed the presence of infected cell clusters consisting of approximately 23.4 ± 8.2 infected cells per cell cluster (Fig. 9B(ii), highlighted by white box). In contrast, anti-G stained lovastatin-treated infected cell monolayers exhibited 2.3 ± 0.9 cells per cell cluster, indicating that lovastatin impaired cell-to-cell transmission of the virus. Similar observations were observed when using anti-RSV to detect the presence of infected cells (Fig. 9C(i)).

Treatment of infected cells with methyl-β-cyclodextrin (MBCD) caused a 60% reduction in cholesterol levels, while cholesterol-methyl-β-cyclodextrin (Ch-MBCD) treatment caused a 60% increase in cholesterol levels (Fig. 4A). Approximately 2.3 ± 0.9 cells per cell cluster was detected in MBCD-treated infected cell monolayers indicating impaired cell-to-cell transmission (Fig. 9B and C(i)). However, cell monolayers treated with Ch-MBCD for 1 h directly after MBCD-treatment showed similar numbers of infected cells per cell cluster to that in non-treated cells (Fig. 9C(ii)). This indicated that cholesterol addition following cholesterol depletion was sufficient to restore virus transmission within the cell monolayer. In contrast anti-RSV labelled lovastatin-treated virus-infected cells treated with ch-MBCD showed a similar number of infected cells/cluster to that in lovastatin-treated cells (Fig. 9D). This further indicated that the additional cholesterol was insufficient to restore cell-to-cell transmission, suggesting that the primary antiviral mode of lovastatin was not due to decreased cholesterol levels. This suggested that other activities associated with HMGCR activity rather than cholesterol biosynthesis play a role in mediating RSV transmission.

4. Conclusion

Our current findings suggested a paradigm shift in the current understanding of RSV morphogenesis and transmission. From a mechanism of virus transmission that involves the release of cell-free virus particles to a mechanism where virus filaments can be viewed as virus-modified cell surface structures that allow the direct transmission of virus cargo (e.g. virus genomes) between infected and non-infected cells. In this context our observations have suggested that virus induced cellular changes leads to cell-to-cell to transmission via actin remodelling. Viruses that are transmitted by direct cell-to-cell contact would have advantages over a predominantly cell-free virus state, for example evasion of the host immune response by HIV-1 (Phillips, 1994; Jolly et al., 2004). Direct cell-to-cell transmission of RSV could avoid the release of the virus particles into a potentially hostile environment of the mucus-coated upper respiratory tract that could potentially

impair virus infection and transmission (Singh et al., 2002). Interestingly, our findings are consistent with previous observations suggesting the localised transmission of RSV in upper airway cells (Zhang et al., 2002). Although our observations differs from that of a recent study (Shaikh et al., 2012), they are consistent with the body of literature suggesting that actin is involved in RSV morphogenesis. During RSV infection a relatively small subset of host genes showed up-regulated gene expression (Martinez et al., 2007; Yeo et al., 2009), suggesting that changes in the cell transcriptome during the early stages of infection may facilitate virus morphogenesis and transmission e.g. by mediating F-actin remodelling. Although future studies will elucidate the molecular mechanisms involved in this process, our current data suggests that virus-induced changes in cellular metabolism mediate RSV transmission. These data also provided a rational basis for the inhibitory action of lovastatin on RSV infection that was reported previously, but which had remained largely uncharacterised (Gower and Graham, 2001).

Acknowledgments

This research was supported by the National Research Foundation Singapore through the Singapore-MIT Alliance for Research and Technology's Infectious Disease IRG research programme. We also thank Duncan McGeoch and the MRC UK for support (GB). The funders had no role in study design, data collection and analysis, decision to publish, or preparation of the manuscript. The authors have no conflict of interest either in the preparation of the manuscript or in the experiments that have been described. Laxmi Iyer Ravi is a recipient of a NTU PhD scholarship (Ministry of Education, Singapore).

References

Bifulco, M., Laezza, C., Aloj, S.M., Garbi, C., 1993. Mevalonate controls cytoskeleton organization and cell morphology in thyroid epithelial cells. J. Cell. Physiol. 155, 340–348.

Bitko, V., Oldenburg, A., Garmon, N.E., Barik, S., 2003. Profilin is required for viral morphogenesis, syncytium formation, and cell-specific stress fiber induction by respiratory syncytial virus. BMC Microbiol. 3, 9.

Brown, G., Rixon, H.W.M., Steel, J., McDonald, T.P., Pitt, A.R., Graham, S., Sugrue, R.J., 2005. Evidence for an association between heat shock protein 70 and the respiratory syncytial virus polymerase complex within lipid-raft membranes during virus infection. Virology 338, 69–80.

Brown, G., Rixon, H.W., Sugrue, R.J., 2002. Respiratory syncytial virus assembly occurs in GM1-rich regions of the host-cell membrane and alters the cellular distribution of tyrosine phosphorylated caveolin-1. J. Gen. Virol. 83, 1841–1850.

Brown, M.S., Dana, S.E., Goldstein, J.L., 1973. Regulation of 3-hydroxy-3-methylglutaryl coenzyme A reductase activity in human fibroblasts by lipoproteins. Proc. Natl. Acad. Sci. 70, 2162–2166.

Burke, E., Dupuy, L., Wall, C., Barik, S., 1998. Role of cellular actin in the gene expression and morphogenesis of human respiratory syncytial virus. Virology 252, 137–148.

Carromeu, C., Simabuco, F.M., Tamura, R.E., Farinha Arcieri, L.E., Ventura, A.M., 2007. Intracellular localization of human respiratory syncytial virus L protein. Arch. Virol. 152, 2259–2263.

Collins, P.L., Hill, M.G., Cristina, J., Grosfeld, H., 1996. Transcription elongation factor of respiratory syncytial virus, a nonsegmented negative-strand RNA virus. Proc. Natl. Acad. Sci. USA 93, 81–85.

Garcia-Beato, R., Melero, J.A., 2000. The C-terminal third of human respiratory syncytial virus attachment (G) protein is partially resistant to protease digestion and is glycosylated in a cell-type-specific manner. J. Gen. Virol. 81, 919–927.

Garcia, J., Garcia-Barreno, B., Vivo, A., Melero, J.A., 1993. Cytoplasmic inclusions of respiratory syncytial virus-infected cells: formation of inclusion bodies in transfected cells that coexpress the nucleoprotein, the phosphoprotein, and the 22K protein. Virology 195, 243–247.

Goldstein, J.L., Brown, M.S., 1990. Regulation of the mevalonate pathway. Nature 343, 425–430.

Gower, T.L., Graham, B.S., 2001. Anti-viral activity of lovastatin against respiratory syncytial virus in vivo and in vitro. Antimicrob. Agents Chemother. 45, 1231–1237.

Gower, T.L., Pastey, M.K., Peeples, M.E., Collins, P.L., McCurdy, L.H., Hart, T.K., et al., 2005. RhoA signaling is required for respiratory syncytial virus-induced syncytium formation and filamentous virion morphology. J. Virol. 79, 5326–5336.

Gower, T.L., Peeples, M.E., Collins, P.L., Graham, B.S., 2001. RhoA is activated during respiratory syncytial virus infection. Virology 283, 188–196.

Grosfeld, H., Hill, M.G., Collins, P.L., 1995. RNA replication by respiratory syncytial virus (RSV) is directed by the N, P, and L proteins; transcription also occurs under these conditions but requires RSV superinfection for efficient synthesis of full-length mRNA. J. Virol. 69, 5677–5686.

Jeffree, C.E., Brown, G., Aitken, J., Su-Yin, D.Y., Tan, B.H., Sugrue, R.J., 2007. Ultrastructural analysis of the interaction between F-actin and respiratory syncytial virus during virus assembly. Virology 369, 309–323.

Jeffree, C.E., Rixon, H.W., Brown, G., Aitken, J., Sugrue, R.J., 2003. Distribution of the attachment (G) glycoprotein and GM1 within the envelope of mature respiratory syncytial virus filaments revealed using field emission scanning electron microscopy. Virology 306, 254–267.

Jolly, C., Kashefi, K., Hollinshead, M., Sattentau, Q.J., 2004. HIV-1 cell to cell transfer across an Env-induced, actin-dependent synapse. J. Exp. Med. 199, 283–293.

Kallewaard, N.L., Bowen, A.L., Crowe Jr., J.E., 2005. Cooperativity of actin and microtubule elements during replication of respiratory syncytial virus. Virology 331, 73–81.

Keyomarsi, K., Sandoval, L., Band, V., Pardee, A.B., 1991. Synchronization of tumor and normal cells from G1 to multiple cell cycles by lovastatin. Cancer Res. 51, 3602–3609.

Koch, G., Benz, C., Schmidt, G., Olenik, C., Aktories, K., 1997. Role of Rho protein in lovastatin-induced breakdown of actin cytoskeleton. J. Pharmacol. Exp. Ther. 283, 901–909.

Levine, S., Klaiber-Franco, R., Paradiso, P.R., 1987. Demonstration that glycoprotein G is the attachment protein of respiratory syncytial virus. J. Gen. Virol. 68 (Pt 9), 2521–2524.

Low, K.-W., Tan, T., Ng, K., Tan, B.-H., Sugrue, R.J., 2008. The RSV F and G glycoproteins interact to form a complex on the surface of infected cells. Biochem. Biophys. Res. Commun. 366, 308–313.

Martinez, I., Lombardia, L., Garcia-Barreno, B., Dominguez, O., Melero, J.A., 2007. Distinct gene subsets are induced at different time points after human respiratory syncytial virus infection of A549 cells. J. Gen. Virol. 88, 570–581.

McCurdy, L.H., Graham, B.S., 2003. Role of plasma membrane lipid microdomains in respiratory syncytial virus filament formation. J. Virol. 77, 1747–1756.

McDonald, T.P., Pitt, A.R., Brown, G., Rixon, H.W.M., Sugrue, R.J., 2004. Evidence that the respiratory syncytial virus polymerase complex associates with lipid rafts in virus-infected cells: a proteomic analysis. Virology 330, 147–157.

Nair, H., Nokes, D.J., Gessner, B.D., Dherani, M., Madhi, S.A., Singleton, R.J., O'Brien, K.L., Roca, A., Wright, P.F., Bruce, N., et al., 2010. Global burden of acute lower respiratory infections due to respiratory syncytial virus in young children: a systematic review and meta-analysis. Lancet 375, 1545–1555.

Osborne, T.F., Gil, G., Brown, M.S., Kowal, R.C., Goldstein, J.L., 1987. Identification of promoter elements required for in vitro transcription of hamster 3-hydroxy-3-methylglutaryl coenzyme A reductase gene. Proc. Nat. Acad. Sci. USA 84, 3614–3618.

Parry, J.E., Shirodaria, P.V., Pringle, C.R., 1979. Pneumoviruses: the cell surface of lytically and persistently infected cells. J. Gen. Virol. 44, 479–491.

Phillips, D.M., 1994. The role of cell-to-cell transmission in HIV infection. AIDS 8, 719–731.

Radhakrishnan, A., Yeo, D., Brown, G., Myaing, M.Z., Iyer, L.R., Fleck, R., et al., 2010. Protein analysis of purified respiratory syncytial virus particles reveals an important role for heat shock protein 90 in virus particle assembly. Mol. Cell. Proteomics, 1829–1848.

Rixon, H.W.M., Brown, G., Aitken, J., McDonald, T., Graham, S., Sugrue, R.J., 2004. The small hydrophobic (SH) protein accumulates within lipid-raft structures of the Golgi complex during respiratory syncytial virus infection. J. Gen. Virol. 85, 1153–1165.

Roberts, S.R., Compans, R.W., Wertz, G.W., 1995. Respiratory syncytial virus matures at the apical surfaces of polarized epithelial cells. J. Virol. 69, 2667–2673.

Santangelo, P., Nitin, N., LaConte, L., Woolums, A., Bao, G., 2006. Live-cell characterization and analysis of a clinical isolate of bovine respiratory syncytial virus, using molecular beacons. J. Virol. 80, 682–688.

Scheid, A., Choppin, P.W., 1977. Two disulfide-linked polypeptide chains constitute the active F protein of paramyxoviruses. Virology 80, 54–66.

Shaikh, F.Y., Utley, T.J., Craven, R.E., Rogers, M.C., Lapierre, L.A., Goldenring, J.R., Crowe Jr., J.E., 2012. Respiratory syncytial virus assembles into structured filamentous virion particles independently of host cytoskeleton and related proteins. PLoS ONE 7, e40826.

Singh, P.K., Parsek, M.R., Greenberg, E.P., Welsh, M.J., 2002. A component of innate immunity prevents bacterial biofilm development. Nature 417, 552–555.

Yeo, D.S.Y., Chan, R., Brown, G., Ying, L., Sutejo, R., Aitken, J., et al., 2009. Evidence that selective changes in the lipid composition of raft-membranes occur during respiratory syncytial virus infection. Virology 386, 168–182.

Yu, Q., Hardy, R.W., Wertz, G.W., 1995. Functional cDNA clones of the human respiratory syncytial (RS) virus N, P, and L proteins support replication of RS virus genomic RNA analogs and define minimal trans-acting requirements for RNA replication. J. Virol. 69, 2412–2419.

Zhang, L., Peeples, M.E., Boucher, R.C., Collins, P.L., Pickles, R.J., 2002. Respiratory syncytial virus infection of human airway epithelial cells is polarized, specific to ciliated cells, and without obvious cytopathology. J. Virol. 76, 5654–5666.